

Manuscript version: Author's Accepted Manuscript

The version presented in WRAP is the author's accepted manuscript and may differ from the published version or Version of Record.

Persistent WRAP URL:

<http://wrap.warwick.ac.uk/150725>

How to cite:

Please refer to published version for the most recent bibliographic citation information. If a published version is known of, the repository item page linked to above, will contain details on accessing it.

Copyright and reuse:

The Warwick Research Archive Portal (WRAP) makes this work by researchers of the University of Warwick available open access under the following conditions.

Copyright © and all moral rights to the version of the paper presented here belong to the individual author(s) and/or other copyright owners. To the extent reasonable and practicable the material made available in WRAP has been checked for eligibility before being made available.

Copies of full items can be used for personal research or study, educational, or not-for-profit purposes without prior permission or charge. Provided that the authors, title and full bibliographic details are credited, a hyperlink and/or URL is given for the original metadata page and the content is not changed in any way.

Publisher's statement:

Please refer to the repository item page, publisher's statement section, for further information.

For more information, please contact the WRAP Team at: wrap@warwick.ac.uk.

Prospects and Challenges of 4H-SiC Thyristors in Protection of HB-MMC-VSC-HVDC Converters

Chengjun Shen¹, Saeed Jahdi¹, Olayiwola Alatise², Jose Ortiz-Gonzalez²,
Avinash Aithal³ and Phil Mellor¹

Abstract—Pole-to-pole DC faults on HB-MMC-VSC-HVDC schemes impose significant risk of cascade failure on IGBT/diode pairs. Other novel topologies with fault blocking capability, i.e. AAC converters, and DC circuit breakers are not yet fully matured. Therefore, silicon thyristors are used to bypass the DC faults until AC breakers activate. However, silicon thyristors are also at risk of failure due to the capacitor voltage collapse at high junction temperatures caused due to imbalanced reverse recovery current conduction. Hence, the recovery cycles are included as part of IEC standard 62501 HVDC type-test program. Emergence of commercial Silicon Carbide (SiC) thyristors has the potential to tackle this risk. This paper investigates such opportunities and challenges by accurately modeling the performance of thyristors at fault. It was seen that SiC thyristors with acceptable surge current and reverse blocking capability can eliminate the failure mode of silicon thyristors due to minimal recovery stored charge, resulting in an equal share of reverse voltage on all thyristors.

Index Terms—Thyristor, Silicon Carbide, HVDC, VSC, Power Semiconductor Devices

I. INTRODUCTION

THYRISTORS are arguably the most rugged power semiconductor devices. They are capable of conducting currents as high as tens of kiloamperes while blocking voltages as high as several kilovolts. These robust characteristics makes them an attractive choice in grid-level applications where such high-voltage high-current features are vital. Although they became commercially available in 1950s by GE, it was not until 1970s that they were first used in a line-commutated high voltage direct current converter (LCC-HVDC) in Canada to replace thyatron valves [1]. In addition to improved efficiency, a key feature which makes them attractive for HVDC is the excellent robustness under high surge currents. The devices used in LCC-HVDC applications typically utilize the entire width of a silicon wafer with diameters up to 6-inch [2]. Nevertheless, there are recent applications, such as grid connection of offshore wind farms, where LCC-HVDC systems cannot be used due to limitations such as inability to operate at weak AC systems. Development of voltage source converters (VSC-HVDC) with hundreds of self-commutated insulated gate bipolar transistors (IGBTs) and capacitors connected in series in early 2000s provided an alternative choice [3]. It is now anticipated that up to

fifty percent of future HVDC projects will be developed by the VSC technology. However, despite all the advantages of VSC-HVDC, the use of IGBTs instead of thyristors subjects the converter to higher risk of cascaded failure in case of over-current transients. Therefore, it is vital to ensure that adequate protection is implemented to avoid catastrophic consequences. To this end, alternative topologies are developed to tackle this shortcoming while DC circuit breakers are also proposed to isolate DC fault [4].

In short, none of these solutions are presently adequately mature. So, parallel thyristors, including press-pack silicon thyristors [5] are currently required to bypass the surge transients from the IGBT/diode pairs, i.e. in the event of a pole-to-pole DC fault on the DC cables. This is currently the most practical protection method despite the additional costs imposed by hundreds of additional thyristors. Operation of silicon thyristors may also result in excessive electro-thermal stress with potential risk of widespread thyristor failures [6].

Recent commercialization of Silicon Carbide (SiC) thyristors has raised speculations on whether using SiC thyristors as a bypass switch has the potential to address the shortcomings of silicon thyristors in protection of VSC units, given the favourable characteristics of SiC thyristors such as low recovery charge and higher junction temperature.

This paper aims to investigate the industrial challenge of unbalanced reverse recovery charge across series-connected silicon thyristors immediately after fault bypass and the possibility of cascaded failure of the thyristors. It will evaluate the characteristics of SiC thyristors under the same scenario and provides a comparative analysis. Section II discusses the characteristics of DC faults; section III discusses the features of state-of-the-art SiC thyristors; section IV discusses the opportunities and challenges of implementation of SiC thyristors in VSC units; section V provides analysis of performance of silicon and SiC thyristors at faults while section VI concludes the paper.

II. MMC-VSC-HVDC CONVERTERS AT DC FAULTS

The initial VSC-HVDC converters had two-level and three-level structures. These were simpler to control, however had many challenges as hundreds of series-connected devices had to be switched simultaneously [3]. They also had poor harmonics, requiring large filters similar to LCC converters. These led to the development of modular multi-level converters (MMC) with isolated voltage-sourced units creating sinusoidal voltages with little, if any, filtering requirement.

The half-bridge (HB) units are shown in Fig. 1.1 are fundamental building blocks of converters. Hundreds of

Manuscript submitted December 12, 2020, revised February 12, 2021, accepted February 15, 2021.

¹ with Department of Electrical Engineering, University of Bristol, UK.

² with School of Electrical Engineering, University of Warwick, UK.

³ with EA Technology, UK.

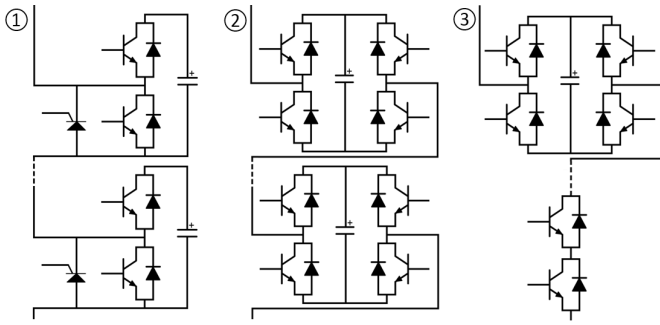


Fig. 1. 1. HB with protective bypass thyristor, 2. FB without the need for a bypass thyristor and 3. Hybrid AAC.

series-connected units with ratings of a few kV each are necessary to support a typical line-to-line voltage of ± 320 kV. As seen, each bottom diode has a parallel protective thyristor [1]–[4], [6] to bypass the fault current due to the lower on-resistance of thyristors compared with diodes. The full bridge unit is shown in Fig. 1.2 with four IGBT modules. This enables them to have a bipolar output by reversing the polarity of capacitor voltage and consequently suppress the DC fault by imposing the significant impedance of charged capacitors in its path. The disadvantages of this topology are higher capital cost and higher losses due to duplicated number of IGBTs. To tackle these shortcomings whilst maintaining the fault blocking capability, a hybrid structure shown in Fig. 1.3, called Alternate Arm Converter (AAC) is proposed [7]. Full-bridge voltage units in this structure conduct only in half of each period controlled by the director switch which constitute series-connection of many individual IGBTs. Therefore, the number of required full-bridge voltage units is halved, so the conduction losses are comparable to that of HB-MMC topology while fault blocking capability is restored. Nonetheless, control of AAC converter is a challenge, in addition to potential DC output ripples when alternating conduction arm. Other topologies are proposed too, most of which are complex. Examples are clamped double cell (CDC), cross connected cell (CCC), and mixed topologies [8].

Fig. 2 shows the HB-MMC-VSC-HVDC converter structure with 6 valves in the 3 phases. The AC breakers promptly interrupt AC side faults while the DC pole-to-ground faults are also manageable by AC breakers due to the significant ground connection impedance. However, a pole-to-pole DC fault, as shown in Fig. 2, imposes a significant risk. Such DC cable fault is rare, however it becomes more likely when overhead lines are used such as in Ultrahigh Voltage Direct Current (UHVDC) project in Germany [9]. The bottom anti-parallel diode provides a low resistance path for the DC fault current to circulate across all bottom IGBT/diode modules. This could result in cascaded failure of devices, especially as the devices initially fail short-circuit as in Fig. 3. Only when the surge current raises further the wire-bonds are destroyed and the short-circuit turns into an open-circuit.

As seen in Fig. 2, there are two types of inductors in the path of the fault current. The first is the arm inductor normally in range of 50 to 100 mH, and the second is the DC line inductor normally in range of 10s of mH. The

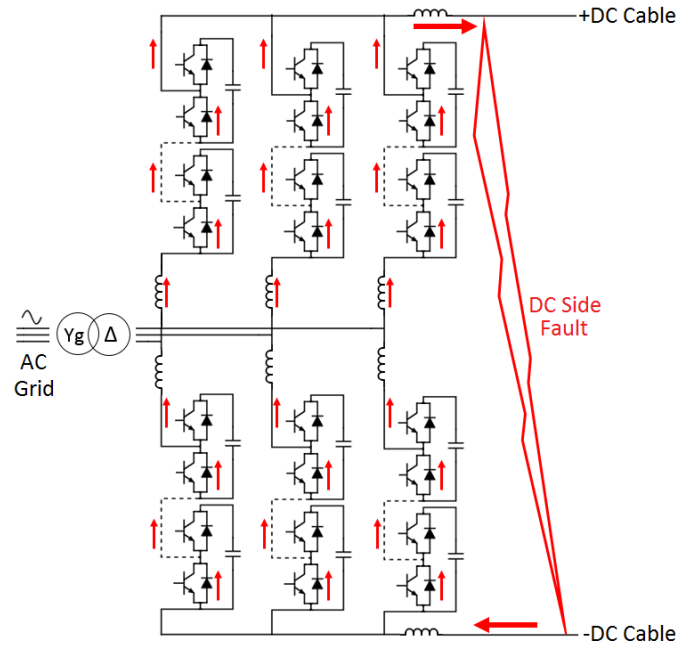


Fig. 2. The pathways for DC fault current in absence of protective bypass thyristors.

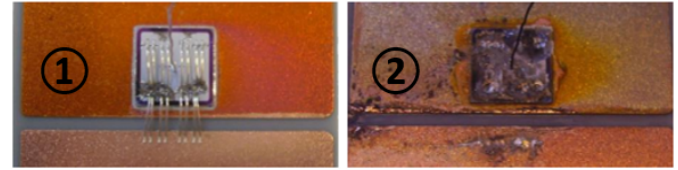


Fig. 3. 1. Short-circuit failure vs. 2. Open-circuit failure of power module wire-bonds [10].

total inductance in fault current's path limits its rate of rise (dI_F/dt) and provide time for current transducers to detect the fault [11], [12]. To interrupt the current, two methods are considered in literature. First, a DC circuit breaker could be initiated [9]. Second, using alternative topologies such as a Full-Bridge (FB)-MMC topology or a hybrid topology like AAC, that reverses the polarity of capacitance voltage in the fault current path. Presently, the DC circuit breakers are still in development, i.e. ABB's first commercial HVDC breaker was introduced in 2012 that required a reaction time of 5 ms [3] while since June 2020, ± 500 kV MMC-HVDC grid with HVDC breakers has been in service in China. These breakers are expensive due to their requirement for series connection of hundred of high voltage devices. Ensuring simultaneous switching of all devices can be complex. In addition, the use of FB-MMC also imposes direct and indirect cost on the design of converter.

Unlike the above-mentioned solutions, a bypass thyristor does not mitigate the fault current but provides a safe bypass path. As indicated in Fig. 4, as soon as the current in each arm reaches a pre-defined value, the thyristors will be fired, and the current is diverted. This transpires in four steps as described as indicated in Fig. 4:

- 1) DC fault occurs and current starts to rise in the diode.

- 2) Current reaches pre-defined value and thyristors fire.
- 3) Fault increases while mostly bypassed in thyristors.
- 4) AC breakers disconnect and converter turns-off.

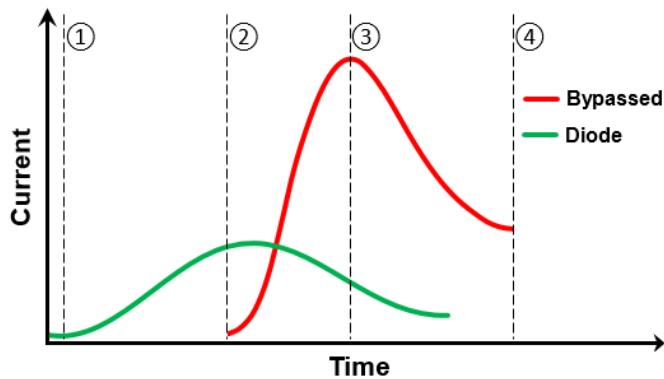


Fig. 4. Fault current bypassed into the protection thyristor.

Thyristors are bipolar devices with some stored charge in space-charge region, especially in silicon devices due to the high carrier lifetime in wider regions. This recovery imposes additional stress on the thyristors. Fig. 5 describes the sequence of events following a fault:

- 1) Initially, all capacitors in the HB-MMC are charged. Some contribute to the overall voltage through the upper IGBTs whilst others are bypassed by bottom diode.
- 2) At instigation of fault, current in the converter arm rises which is fed back to the controllers using current transducers.
- 3) Once the current reaches a pre-defined value, IGBTs turn-off and all thyristors are fired simultaneously. The current flowing through the bottom diodes result in a voltage that forward bias the thyristors. Therefore, the forward blocking capability of thyristors only need to be a few volts while its reverse capability is in the range of few kilovolts. The on-state resistance of thyristors is typically in an order of magnitude that is lower than diodes. The trigger value is set as per the safe operating areas (SOA). The rate of rise of current, turn-on pace of thyristors and communication delays are also considered in the total delay.
- 4) Once the fault is over with AC breakers open, the current in the thyristors drops to turn-off. At this point, the junction temperature of the thyristors is very high due to the surge transient. All bipolar devices start reverse recovery in opposite polarity.
- 5) The diodes have smaller die areas, so their stored charge recovers faster than thyristors which utilize the entire width of a silicon wafer. Therefore, the reverse recovery current continues to conduct only through the thyristors.
- 6) Due to the variations in outputs of production line, there are slight differences in the recovery charge stored in each individual thyristor. Therefore, some thyristors complete the reverse recovery transient while others are still recovering. At this time, the remaining reverse recovery current flows in the upper diode and through the charged capacitor. The forward bias of the upper

diode means that the entire voltage of the capacitor (which up to the moment of fault was at its nominal value) collapses on the thyristor in the reverse polarity, while the thyristor still suffers from a very high junction temperature. This is risky since the thermally-excited carriers have higher mobility and could skip the narrow bandgap of silicon, which could possibly initiate an avalanche breakdown and a potential failure by high electro-thermal stress. This is the rationale of the IEC standard 62501 that requires the recovery voltage between cycles of fault current, including commutation overshoot, to be implemented in protection type-tests. SiC has very low minority carrier lifetime, so SiC thyristors may eliminate this recovery phase altogether.

III. STATE OF THE ART OF SiC THYRISTORS

Challenges in application of silicon thyristors in protection of HB-MMC-VSC-HVDC converters and recent emergence of commercial SiC thyristors have initiated a debate on whether these devices could provide a better alternative to conventional thyristors. The principals that make SiC an attractive choice in fabrication of power devices is extensively discussed [13]–[16]. Many standard and gate turn-off (GTO) SiC thyristors have been developed in recent years. In 2001, 3 kV & 12 A PNP asymmetric SiC super gate turn-off thyristors (SGTO) were introduced [17], [18]. This was followed by development of 4.5 kV SiC SGTO [19], [20], 9 kV SiC SGTO in 2009 [21] and 12 kV SiC thyristor in 2012 [22]. Since then, even higher ratings are demonstrated in laboratories worldwide, i.e. 10 kV 4H-SiC GTO [23], 12.7 kV 4H-SiC commutated gate turn-off thyristor (SICGT) [24], 13 kV SiC emitter turn-off thyristor (ETO) [25], 15 kV SiC ETO [26], 18 kV 4H-SiC thyristor [27], and a 22 kV SiC ETO [28]. Designs for 30 kV SiC thyristors [29], SiC anode switched thyristor (AST) [30], 4H-SiC field-controlled thyristors (FCT) [31] are also available, while 6.5 kV SiC thyristors such as GeneSiC's GA080TH65 are already available in commercial market. The high critical electric field and wide bandgap in SiC are crucial advantages for grid-level heavy-duty power electronics. However, SiC material challenges impact rapid fabrication of devices. The low diffusion length of P-type acceptors has led to absence of thick (~ 1.5 mm) acceptor diffused substrates by ion implantation while the phase vapour transport (PVT) method is currently being used for doping of 4H-SiC substrates. This technique has better yield for the N-type 4H-SiC substrates but it is still problematic for fabrication of the P-type substrates [32]–[38]. Therefore, SiC bipolar devices especially thyristors are made on N-type substrates to avoid excessive substrate resistance. The P-type drift region of devices is not ideal due to the lower mobility of holes compared with electrons resulting in slower transients and higher on-resistance. Recent development of 4H-SiC with lower crystal defect density (compared with 6H-SiC) has made it the preferred polytype, especially when cut at 8 degrees off axis [39]. Higher isotropic mobility of electrons in 4H-SiC ($>200\%$) and higher holes mobility ($>20\%$) are also

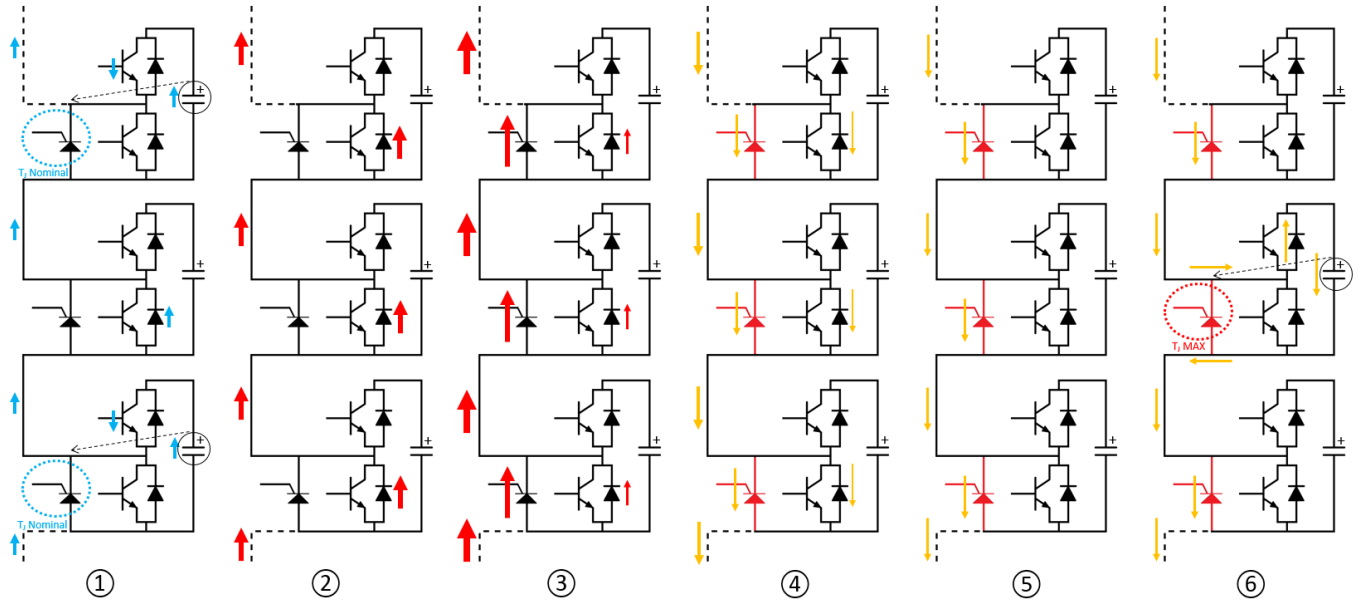


Fig. 5. 1. Normal operation, 2. Instigation of Fault, 3. Thyristors Fired, 4. Fault removed, and devices recover (yellow arrows), 5. All diodes recovered, and Thyristors continue to recover, 6. Some thyristors recovered while others are still recovering.

beneficial. Therefore, commercial SiC thyristors are 4H-SiC NPNP, many of which are ETOs driving the GTO with low voltage MOSFETs, enhancing RBSOA merits. Fig. 6 shows the common structures of silicon and SiC thyristors.

The first type of thyristors in Fig. 6 has a symmetric PNP structure with similar forward and reverse voltage blocking capability which is a common structure in AC power conversion, i.e. LCC-HVDC. The cathode shortings seen in Fig. 6.1 is a feature to increase the forward blocking capability as it delays the avalanche regeneration by reducing the gain of the NPN BJT which has an adverse impact on the base current necessary to maintain the regenerative process especially at higher current levels. Fig. 6.2 shows an NPNP structure with a highly doped thin (a few μm) P-type drift layer to minimize the on-state resistance and avoid a reach-through turn-on. This converts the shape of electric field from triangular into trapezoidal, enabling blocking of higher forward voltage with smaller on-resistance. This structure, however, is unable to withstand any significant reverse voltage as both junctions between the P-anode and N-base and the P-buffer and N-substrate are highly doped and the electric field at the junction rapidly approaches the critical electric field. Fig. 6.3 shows an asymmetric PNP GTO with anode shortings (transparent emitter). The GTO's highly doped P⁺ gate regions assist 'stealing' of the anode current at turn-off. Therefore, applying a reverse polarity voltage on the gate turns off the device. The anode-shorts enable fast turn-off with minimized recovery charge, though eliminating the reverse blocking capability. Finally, Fig. 6.4 shows an asymmetric NPNP GTO with buffer layer as a common 4H-SiC structure with the least on-state resistance and excellent turn-off capability at the price of lack of reverse blocking capability.

Fig. 7 shows typical silicon and SiC thyristors. Silicon thyristors normally utilize the entire width of a wafer, i.e. 2

to 6 inches. In comparison, SiC thyristors, such as GeneSiC Semiconductor's GA080TH65, have lower current ratings with smaller die area due to the difficulties in fabrication of large-area defect-free SiC wafers. The parameters of closely rated Si/SiC thyristors are shown in Table I.

TABLE I
FEATURES OF TWO CLOSELY-RATED SILICON AND SiC THYRISTORS

	4H-SiC	Si
Model	GA080TH65	T201N
Manufacturer	GeneSiC	Infineon
Die Size (mm)	8.2×8.2 of $\varnothing 3''$ disc	$\varnothing 2''$ disc
Forward Voltage (V)	6500	6500
Reverse Voltage (V)	50	6500
RMS Current (A)	139	385
Leakage Current (μA)	50	100000
Reverse Stored Charge (μC)	4	3500
Peak Recovery Current (A)	20	130
Typical Turn-off di/dt (A/ μs)	430	30
Turn-off Time (μs)	10	600
Delay Time (ns)	50	2000
Maximum Temperature ($^{\circ}C$)	150	125
On-state Forward Voltage (V)	3.7	3.4
A-K Slope Resistance ($m\Omega$)	6.33	4.22
A-K Threshold Voltage (V)	3	1.29
J-C Thermal Resistance ($^{\circ}C/W$)	0.08	0.04

Commonly SiC thyristors are SiC p-ETO by connecting P-type SiC GTO to driving MOSFETs. This provides a unity gain turn-off by redirecting the anode current to the gate, rapidly turning it off. It also enables paralleling SiC GTOs for protection of VSCs due to the positive temperature-slope of driving MOSFETs. SiC ETO also has a lower back-porch

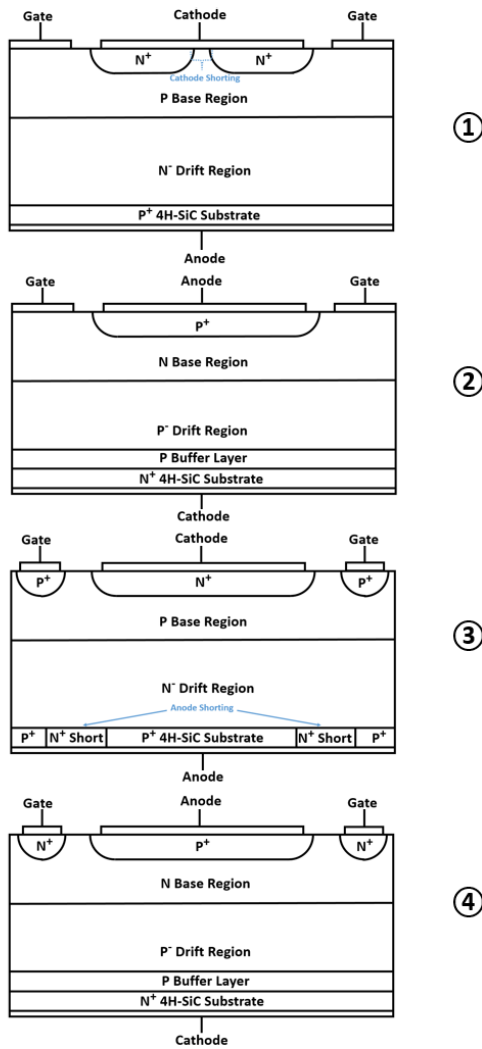


Fig. 6. 1. Symmetric PNP thyristor with cathode shorting, 2. Asymmetric NPN thyristor via buffer layer, 3. Asymmetric PNP SICGT via anode shorting, 4. Asymmetric NPN GTO via buffer layer.

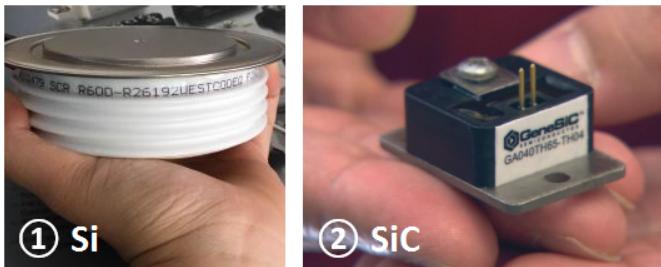


Fig. 7. 1. Typical $\varnothing 4''$ 6.5 kV Silicon thyristor disk, 2. 6.5 kV Silicon Carbide thyristor in SOT-227 package with 8.2×8.2 mm die area cut from a $\varnothing 3''$ 4H-SiC wafer [40].

current requirement compared with silicon GTOs. Several failure modes in thyristors are mitigated by the use of SiC ASTs as:

- 1) Turn-on di/dt : A key failure mode is the rapid increase of current by a high di/dt before the entire width of the wafer or chip conducts. This is less common in silicon GTOs as multiple chips are connected. Commonly, a

turn-on reactor limits the di/dt , however this is not useful in protection of HB units as more current flows into the diode. SiC AST with an involute gate ensures no thyristor failures occurs in absence of this reactor as a result of high turn-on di/dt at DC pole-to-pole faults.

- 2) Turn-off dV/dt : As a thyristor turns-off at end of a fault, the capacitor voltage drops on the device as in Fig. 5. Such dV/dt may result in an unwanted turn-on, leading to failure. This can also happen when a thyristor in forward blocking mode rapidly shifts into reverse blocking, resulting in a substantial displacement current and space-charge shift. A turn-off dV/dt snubber is typically needed. This however, is not required for SiC AST.
- 3) Dynamic Avalanche: At very high-power limits, a dynamic avalanche may take place, resulting in thermal runaway and failure. The power limits in silicon devices is relatively lower, typically about 200-300 kW/cm² [25]. This limit for SiC is so high that other factors, such as packaging temperature limits, will define the SOA.
- 4) Reverse recovery voltage failure on gate-cathode: High reverse recovery coupled with stray inductance causes breakdown by voltage overshoots on the gate-cathode junction. A low recovery charge in SiC eliminates this.

IV. SiC THYRISTORS AS HB-MMC PROTECTION

To this end, the opportunities and challenges for state-of-the-art commercially available SiC thyristors as protection units of HB-MMC-VSC-HVDC converters are:

A. Opportunities

1) *Reverse recovery charge*: The main benefit of application of SiC thyristors is to avoid the failure shown in Fig. 5 by means of enabling simultaneous recovery of all thyristors through negligible stored charge and small recovery current. Silicon GTOs are made of many parallel cells to accelerate the turn-off transient, while SiC single-dies inherently has a low carrier lifetime and rapid recombination of minority carriers. Additionally, its high critical electric field means shorter drift region (i.e. 60 μm for a 10 kV SiC GTO [41] and 160 μm thick for a 22 kV device [42]). This means less carriers over a shorter distance, resulting in a faster recovery. As indicated in Table I, the recovery charge of a silicon thyristor is in range of 3500 μC which is very high in comparison to a 4H-SiC thyristor with just 4 μC . Combining this with the peak recovery current (130 A vs. 20 A) and turn-off time (600 μs vs. 10 μs) means that recovery of SiC thyristors is almost instantaneous. Such short turn-off time also enables it to safely withstand repetitive peaks and zero-crossing of faults.

2) *Junction temperature*: SiC devices are able to operate at higher junction temperatures, as it can maintain its semiconductor properties up to 900°C with melting point of 2700°C. In comparison, narrow bandgap of silicon devices limit junction temperature to 125°C with a melting point of 1400°C, although these are largely restricted by the limitations

on the interface joints between the die and package. Therefore, the maximum junction temperature of silicon thyristor as listed in Table I is 125°C while for SiC thyristors it is 150°C that provides some extra room for operation. Given the wide-bandgap of SiC, high junction temperatures will not impact its blocking capability. The blocking voltage of a typical silicon thyristor at 300°C reduces by a factor of 90% [43] while this reduction for a SiC thyristor is only 4% [44]. Therefore, the likelihood of failure described in Fig. 5 is lower in SiC.

3) *Short turn-on delay time:* The SiC device has shorter delay time in forming the charge required in the N and P regions during turn-on transient due to smaller device area despite same forward voltage blocking. As seen in Table I, the delay time in silicon thyristor is 2000 ns versus 50 ns for the SiC device. However, the impact of this advantage of SiC over silicon may not be significant on the overall reaction time to DC faults when considering the detection and opening times by the ancillary.

4) *Leakage current:* Protection thyristors are permanently connected to the output of HB-MMC voltage units in reverse polarity, so some leakage current is expected. The reverse voltage across the devices in normal conditions is in the range of a few kilovolts. Therefore, the leakage losses of the thyristor must be considered when the total losses of the converter station are calculated, which is in-line with IEC standard 62751. SiC thyristors outperform silicon devices due to the higher energy required by the carriers to reach conduction band. Looking at Table I, in order of magnitude the leakage current of SiC device is three times smaller than that of the silicon devices. Additionally, spurious turn-on due to high junction temperature and reduction of PN junction built-in voltage will not happen in SiC thyristors. The cosmic ray failures in SiC is also 10 times less than that of silicon devices [45]. Although this can be improved in silicon thyristors at the cost of thicker drift regions, it would increase the on-state drop, resulting in higher share of fault current in diode.

B. Challenges

1) *Device structure for reverse blocking:* A key issue in commercial SiC thyristors is its asymmetric structure as in Fig. 6. Although low carrier lifetime in SiC leads to low recovery charge, this impedes adequate conductivity modulation in the drift region in on-state, contributing to additional on-resistance. To enable ample conductivity modulation while maintaining the recovery charge as little as possible, SiC thyristors are designed asymmetrically. Enhancing the carrier lifetime results in a lower forward voltage enabling a better protection of diodes by diverting more current into the thyristor. This will also result in higher reverse recovery charge at turn-off with consequences described in Fig. 5.6. However, HVDC applications need a reverse blocking capability without the reach-through effect, and therefore require a symmetric structure without cathode shortings and with wide epitaxial drift region, such as the one shown in Fig. 6.1. Thyristors used for the protection of HB-MMC are only required to block a few volts in forward

direction (as the forward voltage drop of diode is only needed to forward bias the thyristor into turn-on) while the reverse voltage is in range of a few kilovolts. This is opposite of standard commercial devices. The additional on-resistance as a result of a symmetric structure has no adverse impact on protection of HB-MMC-VSC-HVDC, as the device only turns-on at point of fault. The additional losses is a trade-off for the higher margin in junction temperature of SiC device.

2) *Low current handling capability:* Another significant limitation in the existing commercial SiC thyristors is the low surge current capability. This is mainly due to the high density of micropipe defects in SiC wafers, impeding fabrication of large defect-free SiC discs. Recently, Wolfspeed as a leader in manufacturing of SiC devices, has made substantial progress in reduction of defects and increasing the yield, however the surge current requirements still need purer wafers. This is not a technical limitation, rather a production challenge, and therefore it is deemed that high quality ‘kiloamp rated’ wafers will become available in foreseeable future. This will also assist overcoming the aforementioned challenge in fabrication of symmetric devices with reverse blocking capability as less defects means less recombination traps and higher carrier lifetime, which would subsequently enable fabrication of thinner symmetric devices.

3) *Higher thermal resistance:* The junction-to-case thermal resistance of the SiC device is twice that of silicon, as shown in Table I. This is due to inferior heat transfer capability of the SOT-227 packaging of SiC thyristor compared to silicon disc enclosure which are pressure-connected on one or both sides to heatsink. The higher maximum junction temperature of SiC provides some flexibility in managing this until thyristors with full-scale SiC wafers become available.

V. PERFORMANCE ANALYSIS OF THYRISTORS AT DC FAULTS

To understand the complete scope of improvements offered by 4H-SiC thyristors as fault bypass switches in HB-MMC voltage units, accurate modelings have been performed. Symmetrical voltage blocking was considered based on the principal data indicated in Table I. This was undertaken in the MATLAB blockset of PLECS by PLEXIM, a professional power electronics design tool. Five voltage units are connected in series with each other with a current source acting as the source of fault. Each capacitor in the model is 5 mF and charged with 3 kV. The capacitor voltages are used in the VSC converter to build the full line-to-line DC voltage. At the point of fault, due to the short-circuit on the DC cable, the line-to-line DC voltage drops and is assumed to reach half of the normal operation voltage. Therefore, at point of fault the five voltage units block only 7.5 kV instead of 15 kV. The characteristics of the IGBT and diodes are similar to typical rated commercial devices and are the same in these simulations. Fig. 8.1 shows the peak of fault current on the AC supply side. The peak of fault current is 4 kA while the dI_F/dt at turn-off is 20 A/ μ s. Fault currents may have even more onerous characteristics depending on the fault impedance, with peaks in range of tens of kA with durations as high as hundreds

of milliseconds. Fig. 8.2 shows a comparison of the reverse recovery current of the thyristors upon turn-off. As indicated, the SiC thyristor shows almost no reverse recovery while the silicon thyristor shows a significant reverse recovery current as indicated by variation of stored charge by 20%. This variation in charge can become a potential source of failure.

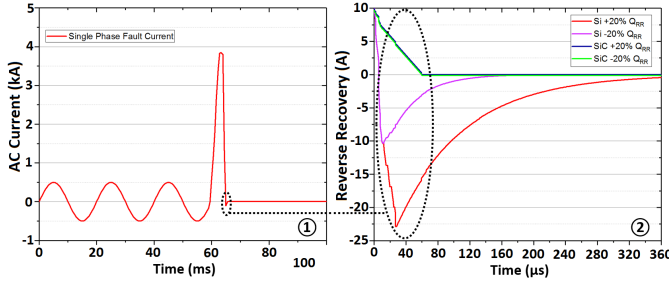


Fig. 8. 1. Synthesized fault current, 2. Reverse recovery current in silicon and SiC thyristor at +20% and -20% charge profiles.

Fig. 9 illustrates the impact of charge variation in the five thyristors by means of imposed reverse voltage on the devices. The variations are in steps of 0.1%, 1% and 10% for both the silicon and SiC devices. Fig. 9.1 shows that the reverse voltage on the silicon thyristors with 0.1% charge variation is constant and all five thyristors share nearly identical reverse voltages of 1.5 kV to block the full converter voltage of 7.5 kV. However, as the variation between the stored charges increase, the reverse voltages also start to vary. The thyristors that have recovered earlier will endure higher voltages compared to those that are still recovering. This reverse voltage is capped at the capacitor voltage; therefore, no thyristor has to endure more than the 3 kV on the capacitor. This is clear in Fig. 9.3 where the reverse voltage on the two thyristors with -10% and -20% charge is clamped at 3 kV. The recovery charge in SiC thyristors is almost negligible, so the variations do not have any impact on the reverse recovery current and therefore the reverse voltage on the thyristors is stable at 1.5 kV in all cases. During normal operation, the thyristors will also be subject to capacitor voltage in the reverse direction. However, this reverse voltage immediately after conduction of fault current occurs at very high junction temperatures and with significant dI/dt and dV/dt which could result in the thyristor failure. This is not the case for SiC thyristor as the reverse voltage at point of reverse recovery is independent of capacitor voltage and solely depends on share of the line-to-line DC voltage which has dropped due to the short-circuit between the DC cables.

In addition to the peak, the time duration that thyristors suffer the reverse voltage should also be considered when selecting the SOA capability. For example, charge variation of 20% results in higher stress compared to 10%, as the duration of the 3kV reverse voltage is prolonged. This is illustrated in Fig. 10 in terms of the V^2t stress of reverse voltage on each device. It is illustrated that by increasing the variation, the stress on the silicon devices also increase, while it remains constant for the SiC device.

Fig. 11 shows the worst-case reverse voltage on the silicon and SiC thyristors with least recovery charge depending on its stored charge. Fig. 11.1 shows that as the recovery charge

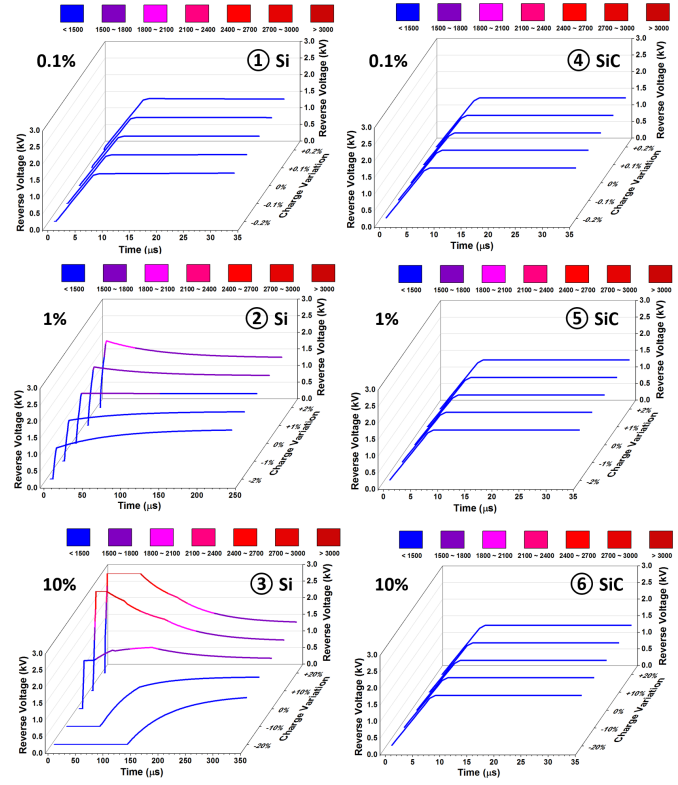


Fig. 9. The reverse voltage depending on recovery charge variations for 1-3. silicon thyristors and 4-6. SiC thyristors.

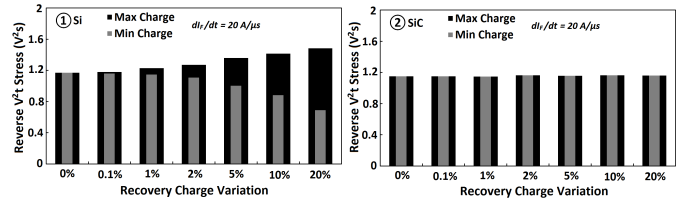


Fig. 10. The V^2t stress on 1. Silicon and 2. SiC device.

variation increases, the peak reverse voltage on the thyristors also increase until it is clamped to the DC capacitor's voltage. It is also seen that with further variation of recovery charge the thyristor has to endure the reverse voltage for a longer period, whilst at highest junction temperature. In comparison, SiC thyristors block the same share of DC line voltage, irrespective of capacitor voltage and charge variations, as shown in Fig. 11.2.

Fig. 12.1 shows similar trends of worst-case reverse voltage for a range of different dI_F/dt . It is shown that similar to the variations in the recovery charge, dI_F/dt also result in different recovery voltages on the thyristors. A similar trend is not seen in the SiC thyristor, due to the fact that the recovery charge indicated by the manufacturer is obtained at the peak turn-off dI/dt capability of the device. Therefore, any lower dI/dt will only result in less recovery charge which further reduces variations in reverse voltage.

A comparison of the impact of peak reverse voltage and dI_F/dt for both Silicon and SiC thyristors was undertaken, under identical conditions. As shown in Fig. 13.1, the peak

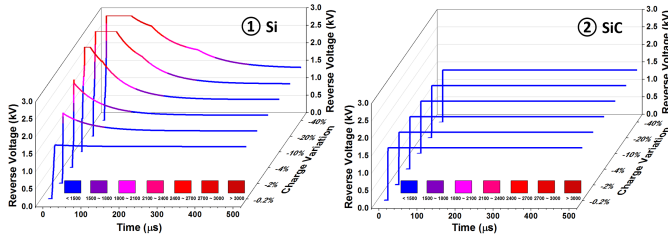


Fig. 11. The worst-case reverse voltage depending on variations of stored recovery charge for 1. silicon thyristors and 2. SiC thyristors.

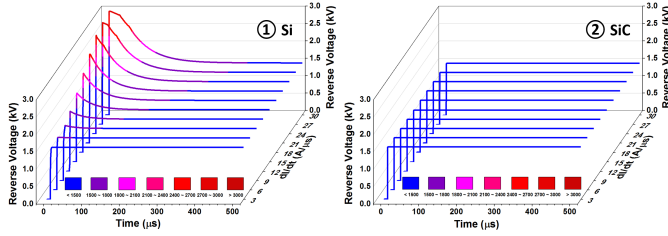


Fig. 12. The worst-case reverse voltage depending on the dI_F/dt rate for 1. silicon thyristors and 2. SiC thyristors.

reverse voltage on the silicon device varies from 1.5 kV to 3 kV over the 0-20% charge variation, while this value remains stable for the SiC thyristor. Fig. 13.2 also shows the significant impact of dI_F/dt on the imposed reverse voltage on the silicon thyristor whilst remaining mostly negligible on the SiC thyristor. Fig. 13.3 and Fig. 13.4 show the electro-thermal stress as a function of V^2t . It is demonstrated that with an increase in the charge variation and dI_F/dt , the electro-thermal stress rises for the silicon device as both the peak reverse voltage and its duration increase. In comparison there is virtually no impact on the SiC device, that suggests a smaller failure-in-time (FIT) rate.

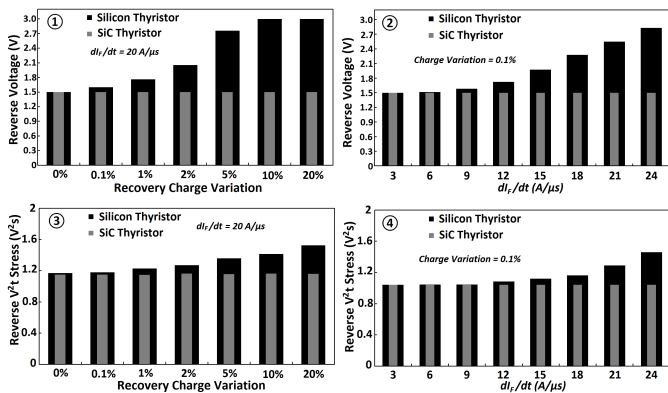


Fig. 13. The worst-case thyristor reverse voltage and V^2t stress indicated by 1 & 3: recovery charge variations and 2 & 4: dI_F/dt .

Fig. 14 shows the 3D plot of modeling results for the silicon device. An increase of both dI_F/dt and charge difference rapidly results in additional reverse blocking requirement on the fast-recovered silicon thyristors. In comparison, the reverse voltage for SiC device consistently remains at its share of DC line-to-line voltage, irrespective of capacitor voltage, charge variation or dI_F/dt .

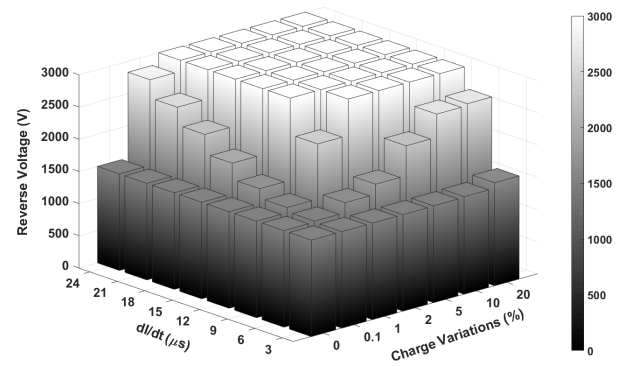


Fig. 14. 3D plot of the worst-case reverse voltage depending on recovery charge variations and fault dI_F/dt of silicon device. N.B., the SiC thyristor reverse voltage is constant at 1.5 kV.

VI. CONCLUSIONS

SiC thyristors can alleviate the electro-thermal stress on the silicon thyristors following bypass of a DC fault current. The ability of SiC thyristors to tackle this stress is predicated upon the low stored recovery charge in the drift region of the device which enables a fast reverse recovery transient. Consequently, the reverse voltage on all thyristors is kept at its minimum, especially when the thyristors suffer from a high junction temperature due to bypassing a significant proportion of surge current. To date majority of SiC thyristors are designed with asymmetrical blocking capability in favour of forward voltage blocking to minimize the on-state voltage drop. In contrast, the reverse blocking capability is the key parameter when used in protection of HB-MMC-VSC-HVDC. Therefore, device structures which are designed in favour of reverse blocking capability are sought. The surge current of the SiC thyristors also need to increase, which would depend on production of defect-free substrates. These are expected to be available in foreseeable future. Therefore, it can be argued that production of high current SiC thyristors with considerable reverse blocking capability will eliminate the main failure risk associated with the use of silicon thyristors and can displace the silicon thyristors and other complex fault management techniques in protection of HB-MMC-VSC-HVDC converters at DC faults.

VII. ACKNOWLEDGEMENT

The authors would like to acknowledge the technical and financial support of the EA Technology® and the EPSRC Supergen Offshore Renewable Energy (ORE) Hub for this research.

REFERENCES

- [1] M. Spence and et al., "Design and characterisation of optimised protective thyristors for vsc systems," in *PCIM Euro.*, May 2016, p. 8.
- [2] B. Li and et al., "A dc fault handling method of the mmc-based dc system," *Int. Jour. Electrical Power Systems*, vol. 93, pp. 39 – 50, 2017.
- [3] M. Barnes and et al., "Voltage source converter hvdc links: State of art and issues going forward," *Energy Procedia*, vol. 24, p. 122, Dec 12.
- [4] G. Tang and et al., "A lcc and mmc hybrid hvdc topology with dc line fault clearance capability," *Jour. Elect. Pow. Syst.*, vol. 62, p. 419, 2014.
- [5] J. Peralta and et al., "Detailed and averaged models for a 401-level mmc-hvdc system," in *IEEE Pow. Ener. Soc. Gen. Meet.*, 2013, pp. 1–1.

- [6] A. Mokherdoran and et al., "Application study of superconducting fault current limiters in meshed hvdc grids protected by fast protection relays," *Electric Power Systems Research*, vol. 143, pp. 292 – 302, 2017.
- [7] M. Merlin and et al., "The alternate arm converter: A new hybrid multilevel converter with dc-fault blocking capability," *IEEE Trans. Pow. Deliv.*, vol. 29, no. 1, pp. 310–317, Feb 2014.
- [8] L. Huang and et al., "The evolution and variation of sub-module topologies with dc-fault current clearing capability in mmc-hvdc," in *Int. Future Energy Electronics Conf.*, June 2017, pp. 1938–1943.
- [9] M. Barnes and et al., "Hvdc systems in smart grids," *Proceedings of the IEEE*, vol. 105, no. 11, pp. 2082–2098, Nov 2017.
- [10] M. A. Eleffendi and et al., "In-service diagnostics for wire-bond lift-off and solder fatigue of power semiconductor packages," *IEEE Trans. on Power Electronics*, vol. 32, no. 9, pp. 7187–7198, Sep 2017.
- [11] U. N. Gnanarathna and et al., "Efficient modeling of modular multilevel hvdc converters (mmc) on electromagnetic transient simulation programs," *IEEE Trans. Pow. Deliv.*, vol. 26, no. 1, pp. 316–324, 2011.
- [12] N. Ahmed and et al., "Efficient modeling of an mmc-based multiterminal dc system employing hybrid hvdc breakers," *IEEE Trans. Pow. Deliv.*, vol. 30, no. 4, pp. 1792–1801, 2015.
- [13] X. She, "Review of sic power devices and their applications," *IEEE Trans. on Industrial Electronics*, vol. 64, no. 10, p. 8193, Oct 2017.
- [14] A. Huang, "Power semiconductor devices for smart grid and renewable energy systems," *IEEE Proceed.*, vol. 105, no. 11, p. 2019, Nov 2017.
- [15] M. Ostling and et al., "State of the art power switching devices in sic and their applications," in *Sil. Nanoelec. (SNW)*, June 2016, p. 122.
- [16] D. Garrido-Diez and et al., "Review of wide bandgap materials and their impact in new power devices," in *ECMSM Workshop*, May 2017.
- [17] S. Ryu and et al., "3100 v, asymmetrical, gate turn-off (gto) thyristors in 4h-sic," *IEEE Elec. Devi. Let.*, vol. 22, no. 3, pp. 127–129, Mar 2001.
- [18] J. B. Fedison and et al., "Switching characteristics of 3 kv 4h-sic gto thyristors," in *58th Device Research Conf.*, June 2000, pp. 135–136.
- [19] Y. Sugawara and et al., "4.5 kv 120a sicgt and its pwm three phase inverter operation of 100kva class," in *Power Semico. Dev.*, June 2006.
- [20] Sugawara and et al., "4.5 kv 60a sicgt and its half bridge inverter operation of 20kva class," in *Power Semico. Dev.*, May 2005, p. 295.
- [21] A. Agarwal and et al., "9 kv, 1 cm sic super gto technology development for pulse power," in *Pulsed Power Conf.*, Jun 2009, pp. 264–269.
- [22] Q. Zhanga and et al., "Sic super gto thyristor technology development: Present status future perspective," in *Puls. Pow. Conf.*, Jun 2011, p. 1530.
- [23] C. Zhou and et al., "10-kv 4h-sic gate turn-off thyristors with space-modulated buffer trench three-step jte," *IEEE Electron Device Letters*, vol. 39, no. 8, pp. 1199–1202, Aug 2018.
- [24] Sugawara and et al., "12.7kv ultra high voltage sic commutated gate turn-off thyristor: Sicgt," in *16th Int. Symp. on Power Semiconductor Devices*, May 2004, pp. 365–368.
- [25] M. A. Rezaei and et al., "Static and dynamic characterization of a 13kv sic p-eto device," in *26th Symp. Power Semic. Dev.*, Jun 2014, p. 357.
- [26] X. Song, "A medium-voltage hybrid dc circuit breaker, part i: Solid-state main breaker based on 15 kv sic emitter turn-off thyristor," *IEEE Jour. Emer. & Sel. Top. Pow. Elec.*, vol. 5, no. 1, p. 278, March 2017.
- [27] S. Rumyantsev and et al., "High current (1225a) optical triggering of 18-kv 4h-sic thyristor in purely inductive load circuit," in *Silicon Carbide and Related Materials 2014*, vol. 821, 7 2015, pp. 893–896.
- [28] X. Song and et al., "Theoretical and experimental study of 22 kv sic emitter turn-off (eto) thyristor," *IEEE Transactions on Power Electronics*, vol. 32, no. 8, pp. 6381–6393, Aug 2017.
- [29] J. Wang and et al., "Feasibility of high voltage sic thyristor in hvdc transmission," in *IEEE PES Conf. (APPEEC)*, Dec 2014.
- [30] S. Sundaresan, "Static and switching characteristics of 6500 v silicon carbide anode switched thyristor modules," in *IEEE Energy Conversion Congress and Exposition (ECCE)*, Sep 2012, pp. 1515–1519.
- [31] R. Singh and et al., "4h-sic buried gate field controlled thyristor," in *55th Annual Device Research Conf.*, June 1997, pp. 34–35.
- [32] M. Bickermann and et al., "Study of boron incorporation during pvt growth of p-type sic crystals," *Mater. Sci. Forum*, vol. 353–356, pp. 49–52, Jan 2001.
- [33] T. Straubinger and et al., "Aluminum p-type doping of silicon carbide crystals using a modified physical vapor transport growth method," *Journal of Crystal Growth*, vol. 240, pp. 117–123, 2002.
- [34] S. Contreras and et al., "Comparative study of p-type 4h-sic grown on n-type and semi insulating 4h-sic substrates," *Mater. Sci. Forum*, vol. 897, pp. 275–278, May 2017.
- [35] M. Zielinski and et al., "P-type doping of 4h- and 3c-sic epitaxial layers with aluminum," *Mater. Sci. Forum*, vol. 858, pp. 137–142, May 2016.
- [36] C. J. Liu and et al., "Progress in single crystal growth of wide bandgap semiconductor sic," *Mater. Sci. Forum*, vol. 954, pp. 35–45, May 2019.
- [37] Y. Sui and et al., "Device options and design considerations for high-voltage (10–20 kv) sic power switching devices," *Mater. Sci. Forum*, vol. 527–529, pp. 1449–52, October 2006.
- [38] T. Abi-Tannous and et al., "A study on the temperature of ohmic contact to p-type sic based on ti3sic2 phase," *IEEE Transactions on Electron Devices*, vol. 63, no. 6, pp. 2462–2468, June 2016.
- [39] E. Tymicki and et al., "Growth of 4h-sic crystals on the 8 degrees off-axis 6h-sic seed by pvt method," *Mate. Sci. For.*, vol. 645, p. 17, Apr 2010.
- [40] R. Singh, "Ultra-high-voltage silicon-carbide (sic) thyristor," *SANDIA National Laboratories*, vol. 100 Research and Development, 2011.
- [41] S. G. Sundaresan and et al., "Large area 8 kv sic gto thyristors with innovative anode-gate designs," in *Silicon Carbide and Related Materials 2009*, vol. 645, Jul 2010, pp. 1021–24.
- [42] X. Song, "Theoretical & experimental study of 22kv sic emitter turn-off thyristor," *IEEE Trans. Pow. Elec.*, vol. 32, no. 8, p. 6381, Aug 2017.
- [43] V. Obreja and et al., "The operation temperature of silicon power thyristors and the blocking leakage current," in *35th Annual Power Electronics Specialists Conf.*, vol. 4, June 2004, pp. 2990–2993.
- [44] T. Burke and et al., "Silicon carbide thyristors for power applications," in *Pulsed Power Conf.*, vol. 1, July 1995, pp. 327–335.
- [45] D. J. Lichtenwalner and et al., "Reliability of sic power devices against cosmic ray neutron single-event burnout," in *Silicon Carbide and Related Materials 2017*, vol. 924, 7 2018, pp. 559–562.



Chengjun Shen received the B.Sc. degree in electronics engineering from the University of York, York, UK, in 2017 and the M.Sc. degree, graduating in electrical engineering from the University of Leeds, Leeds, U.K. in 2018. Since then, he has been working toward the Ph.D. degree in electrical engineering as a PhD candidate in the Electrical Energy Management Group Laboratory, School of Electrical and Electronic Engineering, University of Bristol, Bristol, U.K. His research interests include wide-bandgap semiconductor devices (specifically Silicon Carbide devices) in high voltage power converters, circuits, and high voltage power electronics applications.



Saeed Jahdi (S'10, M'16) received the B.Sc. degree in electrical power engineering from the University of Science and Technology, Tehran, Iran, in 2010, the M.Sc. degree with Distinction in power systems from the City University London, UK, in 2012, and the Ph.D. degree in power electronics from the University of Warwick, UK, in 2016. He was with the HVDC Center of Excellence of General Electric, General Electric (GE) Grid Solutions, Stafford, UK, and is currently an Assistant Professor of Power Electronics with the Electrical Energy Management Group, University of Bristol, UK. His current research interests include wide-bandgap power semiconductor devices in power electronics. Dr. Jahdi is a Chartered Engineer with the IET in the UK.



Olayiwola Alatise (M'19) received B.Eng. (first class Hons.) degree in electrical/electronic engineering and the Ph.D. degree in microelectronics and semiconductors from Newcastle University, Newcastle upon Tyne, U.K., in 2005 and 2008, respectively. In 2004 and 2005, he briefly joined ATMEL North Tyneside where he worked on the process integration of the 130-nm CMOS technology node. In June 2008, he joined the Innovation R&D Department, NXP Semiconductors, as Development Engineer where he designed, processed and qualified discrete power trench MOSFETs for automotive applications and switched-mode power supplies. In November 2010, he joined the University of Warwick as Science City Research Fellow to investigate advanced power semiconductor materials and devices for improved energy conversion efficiency. Since February 2019, he has been a Professor in Electrical Engineering with the University of Warwick, Coventry, U.K. He is the author or co-author of more than 90 publications in journals and international conferences. His research interests include investigating advanced power semiconductor materials and devices for improved energy conversion efficiency. Prof. Alatise is an Associate Editor of the IEEE Journal of Emerging and Selected Topics in Power Electronics.



Jose Ortiz-Gonzalez (S'15, M'18) received a B. Eng. degree in electrical engineering from the University of Vigo, Spain, in 2009, and the Ph.D. degree in power electronics from the University of Warwick, U.K., in 2017. Since 2013, he has been with the School of Engineering, University of Warwick, Coventry, U.K. He was appointed as Senior Research Fellow in Power Electronics in January 2018. Since August 2019, he has been an Assistant Professor in Power Electronics. He has authored or coauthored more than 40 publications in journals and international conferences. His current research interests include electrothermal characterization of power devices, reliability, and condition monitoring.



Avinash Aithal received the B.E. degree in electrical and electronics engineering from the Visvesvaraya Technological University, India, in 2008, M.Sc. degree in Electrical Energy Systems from Cardiff University, UK, in 2013, and a Ph.D. degree in Smart Grids from the Cardiff University, UK, in 2018. He was with the General Electric (GE), Alstom and is currently a Senior Consultant at EA Technology. His current research interest include product development of power electronic devices, integration of smart interventions on electricity networks and techno-economic analysis of future energy networks. He is a Chartered Engineer with the IET in the UK.



Phil Mellor received the B.Eng. and Ph.D. degrees in electrical engineering from the Department of Electrical Engineering, University of Liverpool, Liverpool, U.K., in 1978 and 1981, respectively. He is currently a Professor of Electrical Engineering with the Department of Electrical and Electronic Engineering, University of Bristol, Bristol, U.K. Prior to this, he held academic posts with the University of Liverpool from 1986 to 1990 and the University of Sheffield, Sheffield, U.K., from 1990 to 2000. His current research interests include high-efficiency electric drives and actuation and generation systems for application in more electric aircraft and hybrid electric vehicles.